

Monitoring of tissue coagulation during thermotherapy using optoacoustic technique

Kirill V Larin^{1,4}, Irina V Larina^{1,2} and Rinat O Esenaliev^{1,2,3,5}

¹ Center for Biomedical Engineering, University of Texas Medical Branch, Galveston, TX 77555, USA

² Department of Neuroscience and Cell Biology, University of Texas Medical Branch, Galveston, TX 77555, USA

³ Department of Anesthesiology, University of Texas Medical Branch, Galveston, TX 77555, USA

E-mail: rinat.esenaliev@utmb.edu

Received 30 November 2004, in final form 20 April 2005

Published 22 July 2005

Online at stacks.iop.org/JPhysD/38/2645

Abstract

In this paper we have applied the laser optoacoustic technique for real time noninvasive monitoring of thermal damage in tissues. Changes in tissue optical properties during coagulation were detected by measuring and analysing amplitude and temporal characteristics of optoacoustic signals. Coagulation of liver, myocardium and prostate was induced by interstitial continuous wave Nd:YAG laser irradiation of the samples or by conductive heating. Real time detection of thermally-induced changes in optical properties was performed with sensitive wide-band acoustic transducers. Combination of optoacoustic and diffuse reflectance technique was applied for determination of tissue optical properties: effective attenuation, total diffuse reflectance, reduced scattering coefficient and absorption coefficient. The optical properties did not change up to temperature of coagulation (about 53°C) and sharply increased during heating up to 70°C. Monitoring of the expansion of interstitial coagulation front within freshly excised canine tissues was performed in real time with spatial resolution of about 0.6 mm. The results of our study suggest that this technique can potentially be used for real time precise thermotherapy of malignant and benign lesions at depths of the order of the centimetre.

1. Introduction

Monitoring of tissue optical properties in real time during therapeutic application of heat, or thermotherapy, is required in many surgical procedures. Thermotherapy uses ultrasonic, laser, microwave or radiofrequency radiation as well as other heating agents for destruction of abnormal tissues, including malignant and benign lesions. Monitoring of the tissue coagulation zone in real time can provide selective thermal treatment of benign and malignant lesions with minimal

damage to normal surrounding tissues. Significant difference in optical properties between coagulated and normal tissues can be used to achieve this goal.

Several techniques have been proposed for monitoring of tissue coagulation in real time: magnetic resonance imaging (MRI) (Graham *et al* 1998, Germain *et al* 2002, Weidensteiner *et al* 2003), ultrasound imaging (Fife *et al* 2003, Koch *et al* 2003) and optical tomography (Welch and van Gemert 1995, Lin *et al* 1996, Chin *et al* 2004). Each of these techniques has merits and drawbacks in application to the real time monitoring of tissue coagulation. For example, MRI has high resolution and contrast, but long acquisition time and high cost. Ultrasonography can perform imaging in real time and has relatively low cost. However, it has low

⁴ Present Address: Biomedical Engineering and Mechanical Engineering, University of Houston, Houston, TX 77204-4006, USA.

⁵ Author to whom any correspondence should be addressed.

contrast and sensitivity for coagulation monitoring, because the speed of sound in coagulated tissue is close to that in normal (native) tissue (Techavipoo *et al* 2004). Optical tomography has high contrast owing to dramatic increase of tissue scattering coefficient induced by coagulation, but has poor resolution owing to strong light scattering and attenuation in tissues.

High optical contrast induced in tissue during heating above 52–55°C results from the increase in the scattering coefficient owing to protein denaturation. For example, reduced scattering coefficient, μ'_s , of rat liver increases from 8.25 to 16.2 cm⁻¹ and absorption coefficient, μ_a , decreases from 1.3 to 0.8 cm⁻¹ at the wavelength of 1064 nm owing to coagulation (Essenpreis 1992). At the wavelength of 1320 nm these coefficients are equal to $\mu'_s^{\text{native}} = 2.44$ cm⁻¹, $\mu_a^{\text{native}} = 4.3$ cm⁻¹ and $\mu'_s^{\text{coag}} = 22.8$ cm⁻¹, $\mu_a^{\text{coag}} = 3.6$ cm⁻¹. The reduced scattering coefficient of canine myocardium increases from 4.50 to 9.84 cm⁻¹ at $\lambda = 1064$ nm owing to coagulation, while the absorption coefficient slightly decreases from 0.43 to 0.35 cm⁻¹ (Splinter *et al* 1991). Therefore, coagulation dramatically increases the reduced scattering coefficient and, therefore, the effective attenuation coefficient, μ_{eff} , defined as $\mu_{\text{eff}} = \sqrt{3\mu_a(\mu_a + \mu'_s)}$, while insignificantly altering chemical content or acoustical properties of tissues (Welch and van Gemert 1995).

Laser optoacoustics (OA), a novel imaging modality, was recently proposed for many biomedical applications (recently reviewed by Karabutov *et al* (2003) and Wang (2003) such as breast cancer imaging (Esenaliev *et al* 1999, Kirillov *et al* 1999, Wang *et al* 2002, Andreev *et al* 2003, Copland *et al* 2004), monitoring of oxygenation, total haemoglobin concentration and imaging of blood vessels (Esenaliev *et al* 2002, 2004, Kolkman *et al* 2003), blood glucose sensing (MacKenzie *et al* 1999, Pesach *et al* 2004), and functional and structural imaging of the brain (Wang *et al* 2003a, 2003b, 2004). OA utilizes optical contrast and sensitive detection of laser-induced ultrasonic waves instead of the detection of scattered photons. An advantage of the ultrasonic detection compared with optical detection is that propagation of the acoustic waves in tissues is much less affected by scattering and attenuation than propagation of photon waves. Time-resolved detection of the pressure profiles by ultrasound transducers and analysis of the pressure signals allow for reconstruction of OA images, which resemble distribution of optical inhomogeneities in the irradiated tissue. OA imaging offers a unique possibility of visualizing inhomogeneities deeply in optically turbid and opaque tissues (up to 8 cm in depth) with the axial resolution of 150–500 μm . Therefore, combining the optical contrast between native and coagulated tissues with ultrasound resolution, OA imaging has potential for real time and high-resolution imaging and monitoring of tissue coagulation.

Recently, we applied the OA technique for real time monitoring of the cooling and freezing of tissues (Larin *et al* 2002). The expansion of tissue frozen zone upon application of liquid nitrogen was monitored with a submillimetre spatial resolution and a high contrast. The aims of this pilot study were to demonstrate the capabilities of the OA technique: (1) to detect coagulation-induced changes in optical attenuation between native and coagulated tissues in real time; and (2) to monitor dimensions of coagulated zone in real time during interstitial laser heating.

2. Materials and methods

2.1. Theoretical background

Laser optoacoustic imaging technique is based on thermoelastic mechanism of pressure wave generation (Gusev and Karabutov 1993). Irradiation of an absorbing medium by laser pulses results in local rapid heating and pressure rise. The pressure rise, $P(z)$, in the irradiated volume is dependent on optical and thermophysical properties of the medium and parameters of radiation (Gusev and Karabutov 1993):

$$P(z) = \left(\frac{\beta c_s^2}{C_p} \right) \mu_a F(z) = \Gamma \mu_a F(z) = \Gamma \mu_a F_0 e^{(-\mu_a z)}, \quad (1)$$

where β (°C⁻¹) is the thermal expansion coefficient; c_s (cm s⁻¹) is the speed of sound; C_p (J g⁻¹ °C⁻¹) is the heat capacity at constant pressure; $F(z)$ (J cm⁻²) is the laser fluence; μ_a (cm⁻¹) is the absorption coefficient of the medium. Pressure in (1) can be expressed in J cm⁻³ or in bar (1 J cm⁻³ = 10 bar). The expression $\beta c_s^2 / C_p$ in equation (1) represents the Grüneisen parameter, Γ (dimensionless). The factor $e^{(-\mu_a z)}$ represents exponential attenuation of the optical radiation in the medium.

According to (1), optoacoustic pressure is proportional to the Grüneisen parameter, fluence and absorption coefficient of the medium. If the medium is heterogeneous, equation (1) relates local pressure rise with local Grüneisen parameter, fluence and absorption coefficient. Equation (1) is valid on condition of stress-confinement when pressure relaxation is negligible during the heat deposition. The stress-confined condition is satisfied when the duration of laser pulse, τ_p , is shorter than the stress relaxation time in the irradiated volume, τ_{str} :

$$\tau_p < \tau_{\text{str}} = \frac{1}{\mu_a c_s}. \quad (2)$$

Tissues are strongly scattering media in the ‘therapeutic window’ spectral range (600–1300 nm). In this case, distribution of laser fluence and, therefore, pressure in tissue (not very close to the surface) is dependent on optical absorption and effective attenuation coefficients:

$$P(z) = \Gamma \mu_a k F_0 e^{(-\mu_{\text{eff}} z)}, \quad (3)$$

where k is the parameter that resulted from multiple scattering in tissue and depends on absorption and scattering coefficients (Welch and van Gemert 1995). Accordingly, thermally-induced changes in the optical properties will result in changes in the pressure distribution $P(z)$ during coagulation. The generated stress propagates in all directions from the irradiated volume as a pressure wave and can be detected by an acoustic transducer. Since dimension, z , and time, t , are related by the simple relation $z = c_s t$, the spatial distribution of laser-induced pressure in tissue $P(z)$ is detected by an acoustic transducer as a temporal profile $P(t)$:

$$P(t) = \Gamma \mu_a k F_0 e^{(-\mu_{\text{eff}} c_s t)}. \quad (4)$$

Coagulation-induced changes in tissue optical properties result in changes in spatial (equation (3)) and temporal (equation (4)) optoacoustic pressure profile. Therefore, by recording and analysing the temporal pressure profile, one can monitor dimensions of coagulated zone with high resolution and contrast.

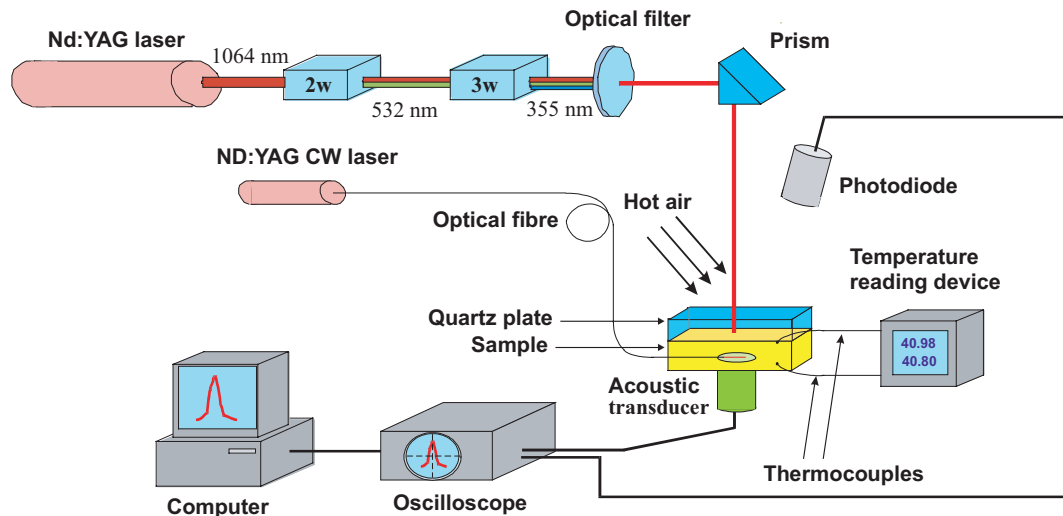


Figure 1. Experimental set-up used in these studies.

(This figure is in colour only in the electronic version)

2.2. Experimental set-up

Experimental set-up utilized in this study is depicted in figure 1. Fundamental ($\lambda = 1064$ nm), second ($\lambda = 532$ nm) and third ($\lambda = 355$ nm) harmonics of Q-switched Nd:YAG laser (Schwartz Electrooptics, Inc.) were used for experiments. The fundamental harmonic was used in most experiments involving tissues because light penetration depth is maximal among these three wavelengths. Some experiments were performed with the fundamental and second harmonics of the laser in order to compare OA contrast for native, coagulated and haemorrhaged tissues in the NIR and visible spectral ranges. The third harmonic was employed for the experiments with model solutions because the dye used in the phantom studies has absorption only in the UV spectral range. To select either of these harmonics, optical filters were inserted in the laser beam. The pulsed laser radiation was directed to the samples using a quartz prism. Energy of each laser pulse was measured with a calibrated joulemeter. Incident laser pulse energy was 15 mJ ($\lambda = 1064$ nm). The laser beam diameter was 6 mm and provided incident laser fluence of 53 mJ cm^{-2} . The laser-induced pressure waves were detected by wide-band acoustic transducers (PZT-transducer (8 MHz) for model solutions and PVDF-transducer (3 MHz) for tissue samples to provide necessary bandwidth for accurate measurements). Transducer signals were recorded by a digital scope (TDS 520, Tektronix Inc.) connected to a PC.

Interstitial tissue coagulation was performed using a continuous wave (CW) Nd:YAG laser (TMED, Inc.) operating at the wavelength of 1064 nm. Output power was varied from 5 to 10 W. The CW laser radiation was delivered through a quartz fibre with a specially designed diffusing tip of 25 mm length. The diffusing tip scattered radiation in 360° resulting in uniform distribution of light with cylindrical symmetry in irradiated tissue. The fibre with the diffusing tip was introduced into the samples through a needle. Such a scheme allowed for interstitial coagulation of a central part of the samples. Before the irradiation the needle was removed from the tissue.

Some experiments were performed using slow conductive tissue heating (the average heating time from 25°C to 70°C was approximately 15 min). Hot air from a heat gun was used to increase temperature in a quartz plate placed on the tissue samples. Direct contact with the quartz plate having good thermal conductivity resulted in uniform conductive heating of the tissue samples. The quartz plate also provided rigid interface for the optoacoustic pressure wave generation (Gusev and Karabutov 1993).

Sample temperature was measured with two thermocouples and a temperature-reading device (ScannerPlus, Azonix Inc.) with an accuracy of 0.3°C . One thermocouple was introduced between the quartz plate and the sample to monitor the upper surface temperature. The other thermocouple was placed either between the sample and acoustic transducer or near the diffusing tip to monitor temperature gradient in the sample.

To measure total diffuse reflectance, R_d , from the samples we used a photodiode (Det 210, Thorlabs, Inc.). The photodiode was positioned at a distance from the sample surface to detect a fraction of total diffuse reflectance (R_d). To provide absolute values of R_d , the photodiode was calibrated using reflectance standards with the total diffuse reflectance of 2%, 20% and 99% (Labsphere, Inc.). The total diffuse reflectance from model solutions and tissues in these experiments was measured by using this calibration (assuming that diffuse reflection from tissues is close to the Lambertian diffuser). Dependence of R_d as a function of μ'_s/μ_a relationship for two refraction indices ($n = 1.33, 1.37$) corresponding to water and tissue, respectively, can be found in (Esenaliev *et al* 1999).

2.3. Phantom

The third harmonic of Nd:YAG laser ($\lambda = 355$ nm) was employed for the experiments with model solutions. Polystyrene microspheres were used to provide scattering, while potassium chromate (K_2CrO_4) was used as an absorber in phantom solutions. The absorption coefficient was measured

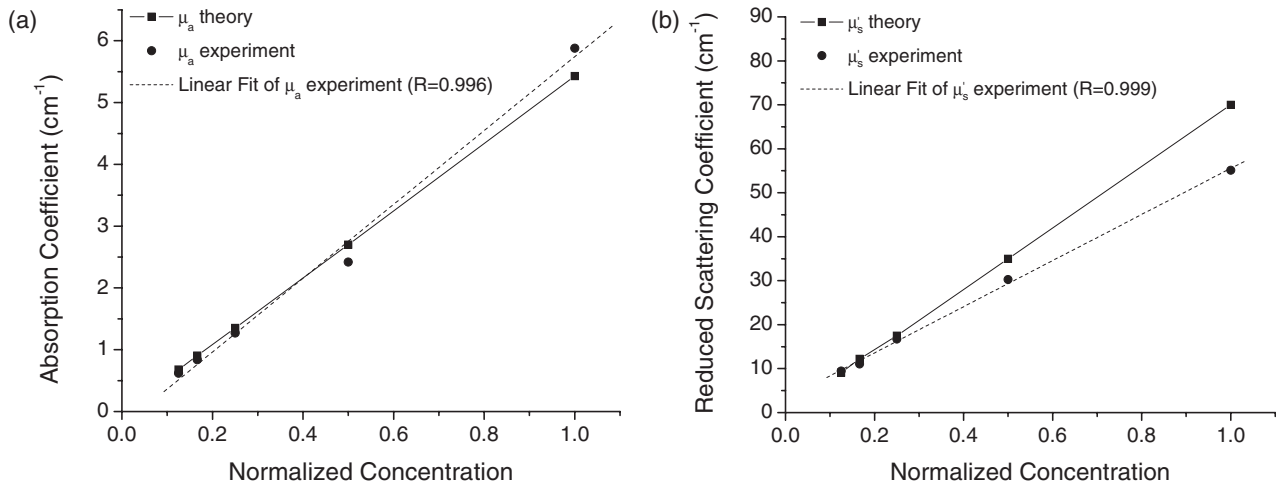


Figure 2. Theoretical and experimental values of absorption (a) and reduced scattering (b) coefficients of tissue phantom at different concentrations.

in clear water solution of K_2CrO_4 from exponential slope of optoacoustic signals. The solutions were placed in a tank with surface area of approximately 50×50 mm (X and Y dimensions) and the phantom thickness was equal to approximately 10 mm (Z dimension). The incident laser beam was directed perpendicular to the top surface of the phantoms and OA signals were detected from the bottom side (the transmission mode). The initial phantom had the following optical properties: absorption coefficient $\mu_a = 5.43 \text{ cm}^{-1}$, scattering coefficient $\mu_s = 769.69 \text{ cm}^{-1}$, anisotropy factor $g = 0.9$ reduced scattering coefficient $\mu'_s = \mu_s(1 - g) = 76.97 \text{ cm}^{-1}$. The scattering coefficient and anisotropy factor were calculated by using the Mie theory (Bohren and Huffman 1983). The experiments were performed with the reference (initial) solution and solutions diluted 2, 4, 6 and 8 times.

2.4. Tissue samples

Freshly excised canine liver, myocardium and prostate tissue were used in our experiments. Slabs with dimensions of approximately 50×50 mm were cut from liver (5 samples) and myocardium (3 samples) tissues. Thickness of the tissue slabs was varied from 8 to 30 mm. The prostate was coagulated *in vivo* 48 h prior to the experiments and cut in 2 mm slices before OA data acquisition. The fundamental and second harmonics of Nd: YAG laser were used to induce OA waves in the tissue samples. The experiments were performed at room temperature ($\sim 20^\circ\text{C}$).

Slow conductive heating of tissues was performed up to a temperature of 70°C . The tissue samples were placed on the transducer and covered from the other sides by a thin plastic film to avoid dehydration during the heating. Data acquisition was performed for 1 s at 1 min intervals in the experiments with CW laser interstitial coagulation. The repetition rate of the pulsed laser radiation was 10 Hz, which allowed averaging of 10 pressure wave profiles during acquisition time. Continuous data acquisition was performed during experiments with slow conductive heating.

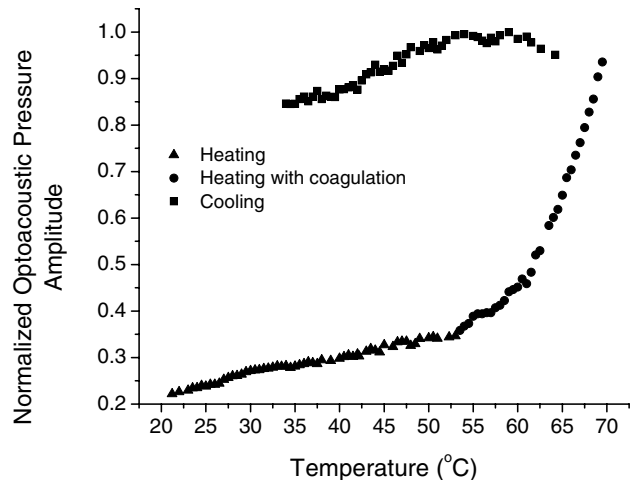


Figure 3. Optoacoustic pressure amplitude induced in canine liver during conductive heating and passive cooling. The triangles (\blacktriangle) represent heating without coagulation; circles (\bullet)—heating with coagulation; squares (\blacksquare)—passive cooling of the sample.

3. Results

Figure 2 shows theoretical and calculated absorption and reduced scattering coefficients of the solutions as a function of concentration. To obtain these data, the OA pressure profiles were measured to calculate the effective attenuation coefficient using equation (4). Then these data were combined with total diffuse reflectance measurements to calculate the absolute values of the absorption and reduced scattering coefficients of the phantoms (the same approach was used for tissues). The total diffuse reflectance was equal to 0.37 for all the solutions because the ratio μ'_s/μ_a does not change with dilutions.

Typical OA peak pressure amplitude induced in the canine liver versus temperature is presented in figure 3. The measurements were performed in real time during conductive heating and passive cooling of the tissue sample. Since the tissue was heated very slowly, the difference between readings of two thermocouples was no more than

1–2°C (the average temperature is indicated in figures 3–5). The amplitude of optoacoustic signal increased linearly with the increase in the temperature from 22°C to about 53°C. The increase in the OA signal amplitude in this range was due to the increase in the Grüneisen parameter, not the optical properties of the tissue (see, equation (4)). Changes in optical properties of tissue induced by coagulation resulted in a sharp increase of the pressure amplitude on heating from 53°C to 70°C. When the tissue temperature reached 70°C, the heating was ceased and the tissue temperature decreased owing to passive cooling. The pressure amplitude continued to increase during the passive cooling from 70°C to 54–52°C owing to the continued tissue coagulation. Passive cooling below 50°C resulted in a gradual decrease in the pressure amplitude.

The exponential slope of optoacoustic pressure induced in a liver sample was measured as a function of temperature (figures 4(a)–(c), solid curve). It was constant up to the temperature of 53°C (figure 4(a)), dramatically increased at higher temperatures (figure 4(b)) and was relatively constant during the passive cooling (figure 4(c)). At a temperature of 70°C the slope measured from the coagulated tissue was approximately two times greater than that measured from normal liver. The total diffuse reflectance (figure 4(a)–(c), dashed curve) from the liver tissue did not change at low temperatures as well (figure 4(a)). The sharp rise of the slope and R_d (figure 4(b)) was possibly caused by a dramatic increase in tissue scattering coefficient owing to protein denaturation (Welch and van Gemert 1995).

Figure 5 depicts optoacoustic pressure amplitude and slope versus temperature for canine myocardium samples during conductive heating. The amplitude increased slowly, while the slope was constant up to the temperature of about 55°C. The sharp increase in both parameters was detected at the temperatures above 55°C. These steep increases are likely to be associated with the rapid changes in the scattering coefficient in the course of the coagulation process.

Pressure profiles recorded in real time during interstitial coagulation at the laser power of 7 W for 6 min are shown in figure 6(a). The change in the OA signal profile during CW irradiation indicates changes in optical properties in the sample due to coagulation. Arrows indicate the position of coagulation zone edge at 0, 2, 5 and 6 min after the onset of irradiation. The delay between the edge and the signal from the diffusing tip is equal to 3.3 μs and 4.7 μs at the irradiation time of 2 min and 6 min, respectively. One can calculate the distance between the diffusing tip and the outer boundary of coagulated zone by multiplying the temporal delay by speed of sound in the coagulated tissue. This distance is the half-width of the coagulated zone. The speed of sound measured in the native and coagulated samples was 1.52 $\text{mm } \mu\text{s}^{-1}$ and 1.54 $\text{mm } \mu\text{s}^{-1}$, respectively (data not shown). Figure 6(b) depicts expansion of the coagulated zone during coagulation calculated from experiments on three liver samples. Rapid expansion of the coagulated zone occurred for the first two minutes. Afterwards, the coagulated zone expansion was substantially slower. Figure 6(c) shows a gross picture of a sample after CW irradiation at the power of 7 W for 6 min obtained immediately after the experiment. In the central part of the sample there is a coagulated zone (light area) with a trace from the diffusing tip. The measured width of the coagulation

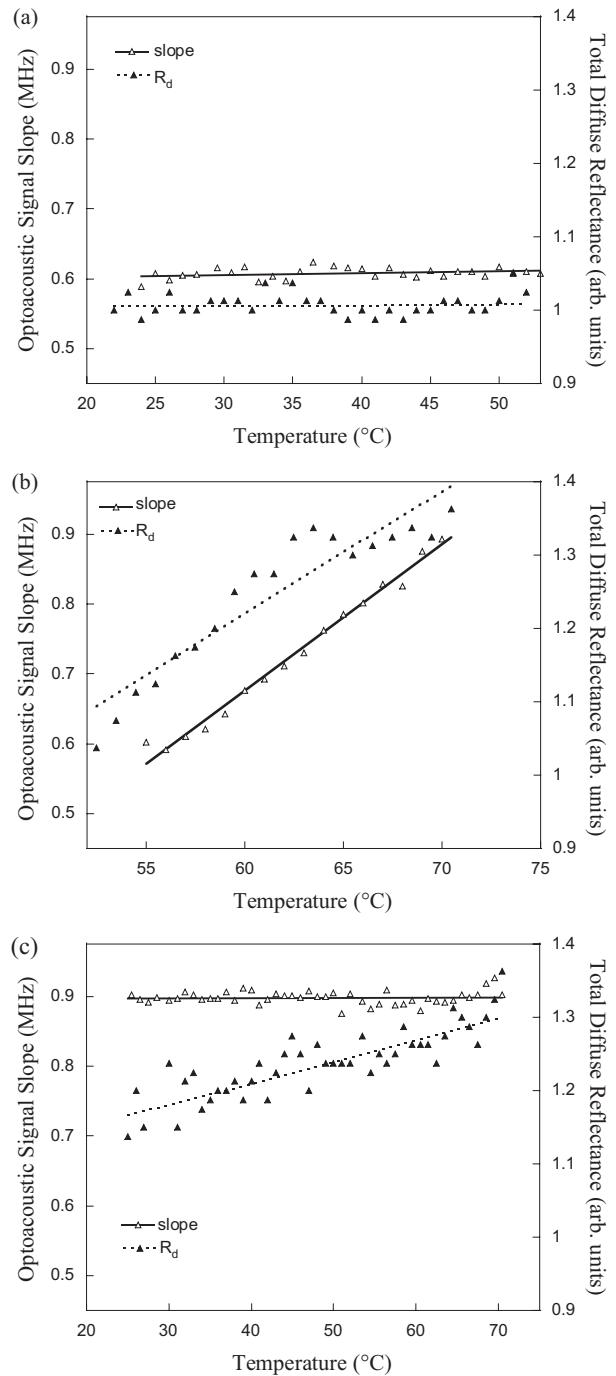


Figure 4. Optoacoustic signal slope and total diffuse reflectance measured from canine liver during: (a) heating without coagulation; (b) heating with coagulation; and (c) passive cooling.

zone is 14.0 mm. This value is in good agreement with the value of 14.6 mm calculated from optoacoustic pressure profile recorded at the end of CW irradiation (see figure 6(b)).

Optoacoustic signals recorded from native and coagulated tissues as well as from the haemorrhage ring of the canine prostate at the wavelengths of 1064 and 532 nm are presented in figures 7(a) and (b), respectively. The first peaks in the figure 7(a) represent optoacoustic pressure induced in the acoustic transducer irradiated by laser light transmitted through these three layers. Owing to strong attenuation of green

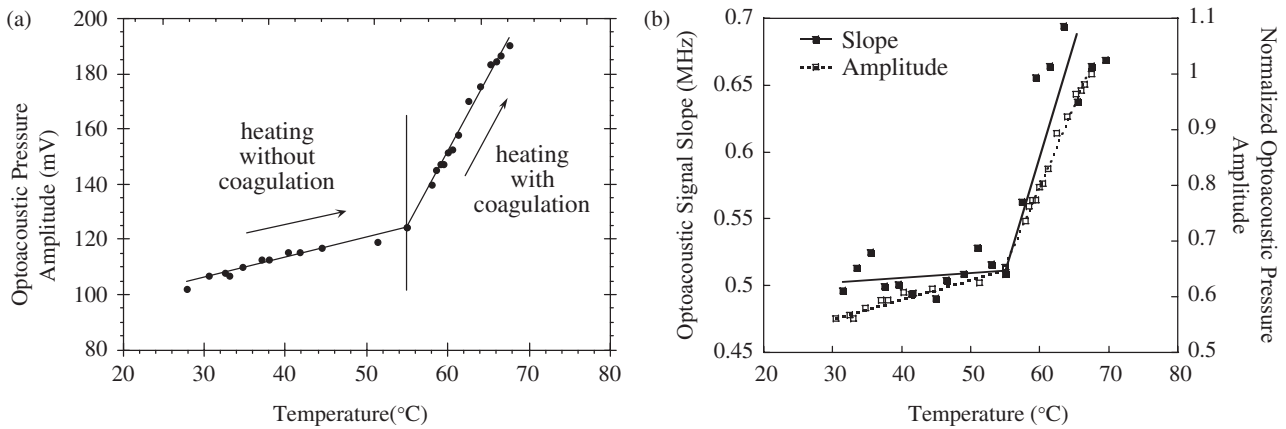


Figure 5. Optoacoustic pressure amplitude (a) and slope (b) versus temperature for canine myocardium samples during conductive heating.

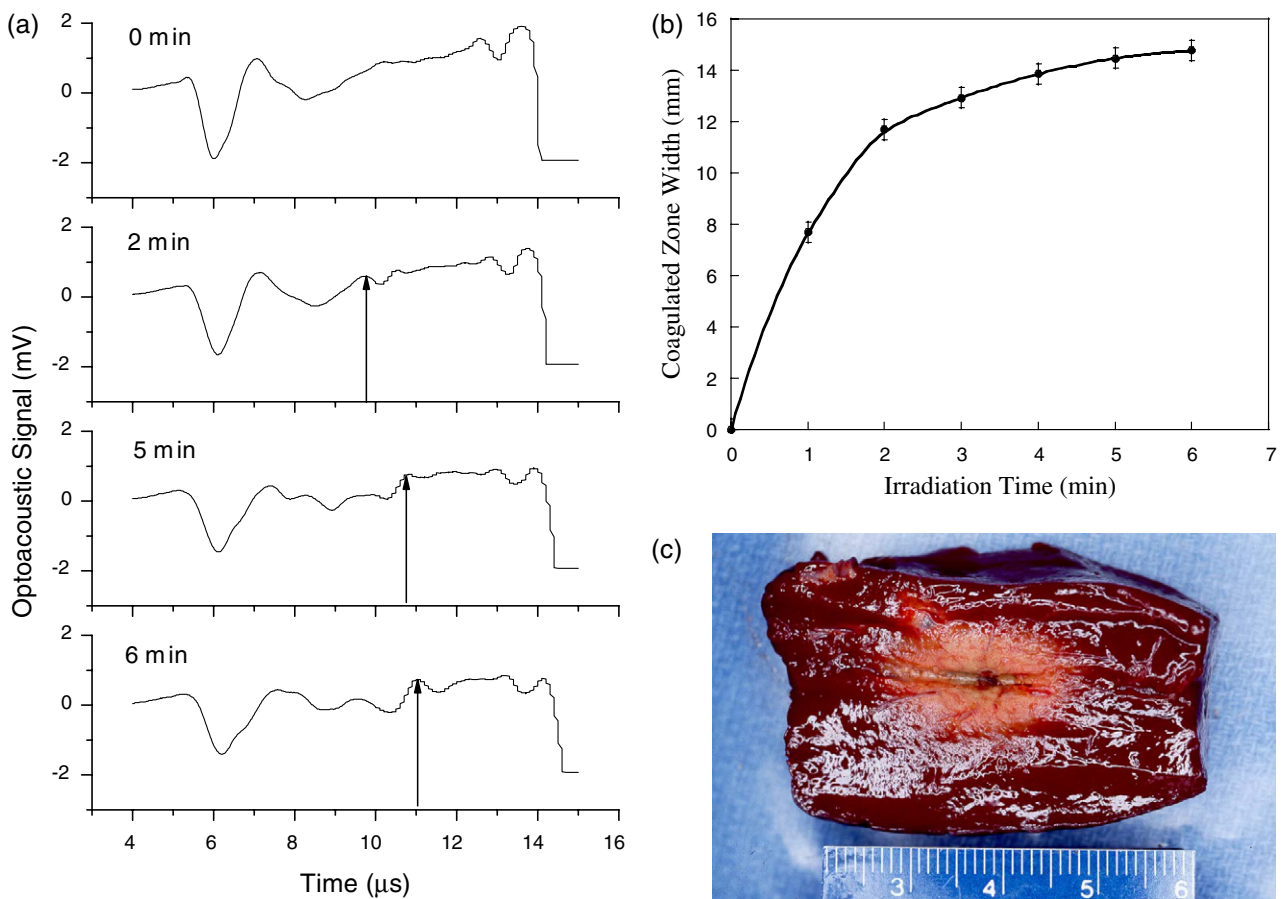


Figure 6. (a) Optoacoustic pressure profiles recorded 0, 2, 5 and 6 min after the onset of CW laser irradiation with the power of 7 W in the canine liver tissue. The arrows indicate the position of coagulated front at different times during radiation and position of the diffusing tip. (b) Coagulated zone width versus irradiation time (the standard deviation was calculated from five independently measured OA signals for the same tissue temperature). (c) Gross picture of the liver tissue obtained immediately after experiments (scale is in centimetres). (This figure is in colour only in the electronic version)

light in tissues, no optoacoustic pressure was induced in the acoustic transducer upon irradiation of the sample by the second harmonic of Nd:YAG laser (figure 7(b)). The second peaks were pressure signals induced at the irradiated tissue surfaces. One can clearly see that the haemorrhage ring and coagulated tissues produce optoacoustic pressure with greater amplitude than native tissue.

4. Discussion

Our experiments with model solutions demonstrate good agreement between the theoretically calculated and experimentally obtained values of absorption coefficient (the average deviation between theoretical and experimental data is 8% and is nearly constant in the studied range). In contrast,

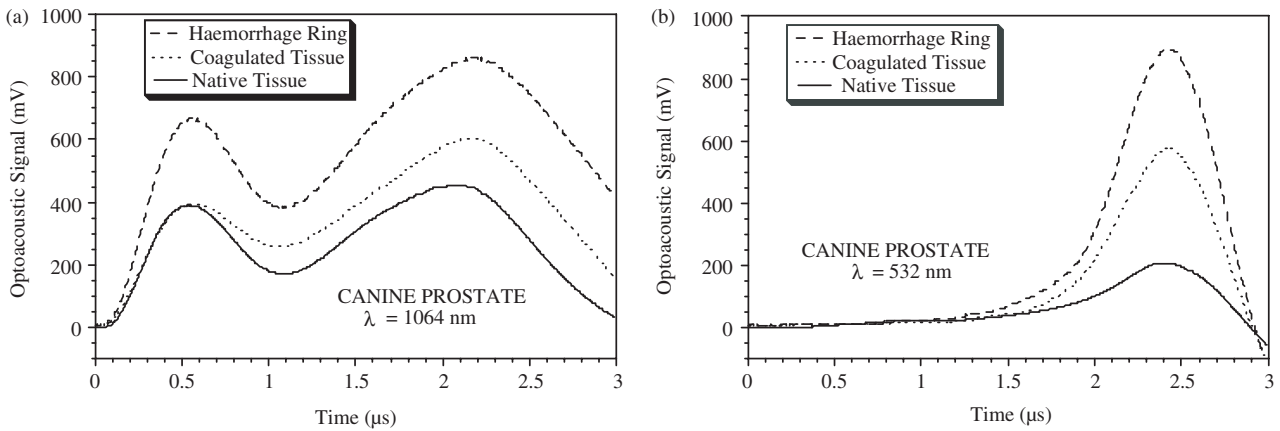


Figure 7. Optoacoustic contrast between native tissue, coagulated tissue and haemorrhage ring of the canine prostate at the wavelength of 1064 nm (a) and 532 nm (b).

Table 1. Optical properties of native and coagulated canine tissues measured with the OA and total diffuse reflectance techniques.

Tissue	R_d	$\mu_{\text{eff}} \text{ (cm}^{-1}\text{)}$	$\mu_a \text{ (cm}^{-1}\text{)}$	$\mu'_s \text{ (cm}^{-1}\text{)}$
Native liver	0.37 ± 0.01	3.59 ± 0.27	0.53 ± 0.03	7.56 ± 0.92
Coagulated liver	0.46 ± 0.05	6.51 ± 1.87	0.71 ± 0.30	19.9 ± 6.2
Native myocardium	0.45 ± 0.01	1.84 ± 0.06	0.20 ± 0.01	5.35 ± 0.34
Coagulated myocardium	0.54 ± 0.05	4.96 ± 0.70	0.39 ± 0.05	21.1 ± 6.1

good agreement between theoretical and experimental values of reduced scattering coefficient was observed only for small values of μ'_s (deviation is 4%), while they significantly differ at high values of μ'_s (maximal deviation is 21%). This discrepancy at high values of μ'_s is possibly due to: (1) the finite size of the tank used in the experiments (the diffusion theory in its simplest form assumes an infinite medium), and (2) difference between the diffuse reflectance from the sample and ideal Lambertian diffuser. Nevertheless, these data demonstrate that one can measure the absorption and scattering coefficients that are typical for tissues in NIR spectral range by using a combination of diffuse reflectance and optoacoustic techniques with accuracy of several per cents.

The calculated values of total diffuse reflectance, effective attenuation, absorption and reduced scattering coefficients for the native and coagulated canine liver tissues are summarized in table 1. One can see that all these parameters increase owing to tissue coagulation. These results are in good agreement with previously reported data (Essenpreis 1992).

The experimental studies in canine tissues demonstrated the increase in optoacoustic pressure amplitude with tissue heating (figures 3 and 5). This increase has two well-distinguished phases: relatively slow increase up to a temperature of about 53°C and a sharp increase of pressure amplitude at higher temperatures. The first phase is due to the changes in thermophysical properties of the tissue (thermal expansion coefficient, speed of sound and heat capacity at constant pressure) that results in a gradual increase in the Grüneisen coefficient or efficiency of optoacoustic wave generation. The increase in the efficiency of pressure wave generation in water was observed upon irradiation by laser pulses with high fluencies and is referred to as thermal nonlinearity of optoacoustic pressure generation (Gusev and Karabutov 1993). The effect results mainly from the increase

in water thermal expansion coefficient with the temperature (Weast 1974, Kikoin 1976).

The effect of optoacoustic pressure amplitude increase with temperature can be applied for monitoring of tissue temperature during hyperthermia. There is approximately 1.5% per 1°C increase in pressure amplitude (9% increase if the liver is heated from 37°C to 43°C). These results indicate that one can monitor temperature rise in tissues by detecting the pressure wave amplitude with an accuracy of about 1°C (Larina *et al* 2005).

The increase in pressure amplitude with the temperature is noticeable and substantially greater than changes in acoustic properties (speed of sound and density) and chemical content of the tissue. This may result in improved contrast of optoacoustic images as compared with other imaging modalities.

The sharp increase in pressure amplitude during tissue heating from 53°C to 70°C is caused mainly by a dramatic increase of tissue scattering coefficient due to coagulation (figures 3 and 5). The potential increase in Grüneisen coefficient in this temperature range may contribute to the increase in optoacoustic pressure amplitude also.

The slope of the optoacoustic signal, $\mu_{\text{eff}} c_s$, (equation (4)), obtained from the liver tissue did not change up to a temperature of about 53°C and sharply increased during heating up to 70°C. This is due to changes in tissue optical properties at temperatures above 53°C. The increase is caused mainly by the dramatic changes in scattering coefficient owing to tissue coagulation. The increase in absorption coefficient also contributes to the changes in the slope.

The formation of the sharp edge in the OA pressure profiles was due to the increase in the attenuation coefficient of the coagulated zone (figure 6(a)) and was used for measurements of coagulated zone dimensions and its expansion as a function of time. The propagation of the edge was manually monitored

and measured for all the OA signals. The comparison of AO signals recorded during the coagulation process enabled us to reveal the time-dependent location of the edge (in future studies we plan to develop automatic processing algorithms to extract the edge location as a function of time). Rapid expansion of the coagulated zone was observed during the first two minutes of irradiation followed by a slower expansion rate. This dynamics is typical for tissue coagulation and was noticed by other researchers as well (Thomsen 1995). The width of the coagulated zone measured using the optoacoustic technique is in good agreement with that measured from the gross picture (14.6 mm and 14.0 mm, respectively). Therefore, one can conclude that the dimensions of coagulated zone can be monitored with submillimetre axial resolution.

Experiments with the prostate demonstrated high optoacoustic contrast between native and coagulated tissues and haemorrhage ring. The optoacoustic pressure signals measured from the coagulated prostate tissue are greater than those measured from the native tissue. This is due to the increased scattering coefficient of coagulated prostate tissue compared with that of the native tissue. The greater amplitude of optoacoustic pressure induced in the haemorrhage ring is explained by the increased absorption due to the higher blood content. The haemorrhage ring is induced in real time in various tissues during *in vivo* coagulation and indicates the outer boundary of thermally-induced lesions (Thomsen 1995, Welch and van Gemert 1995). Therefore, the high optical contrast between these three tissue states (native, coagulated and haemorrhage ring) can be used for precise, real time monitoring of tissue coagulation *in vivo* by the optoacoustic technique.

5. Conclusion

Our studies demonstrated that the optoacoustic technique is capable of sensitive detection of thermally-induced changes in tissue optical properties in real time at depths of up to three centimetres and *z*-axial monitoring of coagulated zone dimensions in real time with submillimetre resolution. The coagulation-induced changes were monitored by analysing the OA signal profiles. In our other work, we also demonstrated that moderate temperature rise in tissues (before coagulation, or, when the tissue optical properties remain constant) might be monitored by analysing OA signal amplitude (Larina *et al* 2005). Therefore, a combination of these two methods may result in the development of a noninvasive modality for the monitoring of thermotherapy in tissues.

In addition, the optoacoustic monitoring is a minimally invasive technique because laser pulses applied for thermoelastic wave generation have low energy and cannot induce thermal or mechanical damage to irradiated tissues. We believe that this technique may become a widely applied tool for real time monitoring of coagulation of malignant and benign lesions because the heating agents (radiofrequency, microwave, ultrasonic or laser radiation as well as conductive and convective heating) do not influence the detection and data acquisition of optoacoustic signals. However, extensive *in vivo* animal and human studies should be performed to validate this technique.

Acknowledgments

The authors thank Dr Chanjie Yang and Brent Bell for technical assistance and the Whitaker Foundation for supporting these studies.

References

- Andreev V G, Karabutov A A and Oraevsky A A 2003 Detection of ultrawide-band ultrasound pulses in optoacoustic tomography *IEEE Trans. Ultrason. Ferroelectr. Freq. Control* **50** 1383–90
- Bohren C F and Huffman D R 1983 *Absorption and Scattering of Light by Small Particles* (New York: Wiley)
- Chin L C L, Wilson B C, Whelan W M and Vitkin I A 2004 Radiance-based monitoring of the extent of tissue coagulation during laser interstitial thermal therapy *Opt. Lett.* **29** 959–61
- Copland J A, Eghtedari M, Popov V L, Kotov N, Mamedova N, Motamedi M and Oraevsky A A 2004 Bioconjugated gold nanoparticles as a molecular based contrast agent: implications for imaging of deep tumors using optoacoustic tomography *Mol. Imag. Biol.* **6** 341–9
- Esenaliev R O, Karabutov A A and Oraevsky A A 1999 Sensitivity of laser opto-acoustic imaging in detection of small deeply embedded tumors *IEEE J. Selected Top. Quantum Electron.* **5** 981–8
- Esenaliev R O, Larin K V, Larina I V, Motamedi M and Oraevsky A A 1998 Optical properties of normal and coagulated tissues: measurements using combination of optoacoustic and diffuse reflectance techniques *Proc. SPIE* **3726** 560–6
- Esenaliev R O, Larina I V, Larin K V, Deyo D J, Motamedi M and Prough D S 2002 Optoacoustic technique for noninvasive monitoring of blood oxygenation: a feasibility study *Appl. Opt.* **41** 4722–31
- Esenaliev R O, Petrov Y Y, Hartrumpf O, Deyo D J and Prough D S 2004 Continuous, noninvasive monitoring of total hemoglobin concentration by an optoacoustic technique *Appl. Opt.* **43** 3401–7
- Essenpreis M 1992 Thermally induced changes in optical properties of biological tissues *PhD Thesis* University College London
- Fife S, Andereck C D and Rahal S 2003 Ultrasound thermometry in transparent and opaque fluids *Exp. Fluids* **35** 152–8
- Germain D, Vahala E, Ehnholm G J, Vaara T, Ylihautala M, Savart M, Laurent A, Tantu J and Saint-Jalmes H 2002 MR temperature measurement in liver tissue at 0.23 T with a steady-state free precession sequence *Magn. Reson. Med.* **47** 940–7
- Graham S J, Bronskill M J and Henkelman R M 1998 Time and temperature dependence of MR parameters during thermal coagulation of ex vivo rabbit muscle *Magn. Reson. Med.* **39** 198–203
- Gusev V E and Karabutov A 1993 *Laser Optoacoustics* (New York: AIP)
- Karabutov A A, Savateeva E V and Oraevsky A A 2003 Optoacoustic tomography: New modality of laser diagnostic systems *Laser Phys.* **13** 711–23
- Kikoin I K 1976 *Tables of Physical Parameters* (Moscow: Atomizdat)
- Kirilov A G, Lozhkarev V V, Mansfel'd A D, Reiman A M, Friedman G I and Yakovlev I V 1999 Application of quasi-resonant ultrasonic detectors in the optoacoustic tomography of biological objects *Quantum Electron.* **29** 832–5
- Koch C, Friedrich T, Metternich F, Tannapfel A, Reimann H P and Eichfeld U 2003 Determination of temperature elevation in tissue during the application of the harmonic scalpel *Ultrasound Med. Biol.* **29** 301–9
- Kolkman R G M, Hondebrink E, Steenbergen W and De Mul F F M 2003 In vivo photoacoustic imaging of blood vessels using an

- extreme-narrow aperture sensor *IEEE J. Selected Topics Quantum Electron.* **9** 343–6
- Larin K V, Larina I V, Motamedi M and Esenaliev R O 2002 Optoacoustic laser monitoring of cooling and freezing of tissues *Quantum Electron.* **32** 953–8
- Larina I V, Larin K V and Esenaliev R O 2005 Real-time optoacoustic monitoring of temperature in tissues *J. Phys. D: Appl. Phys.* **38** 2633
- Lin W C, Motamedi M and Welch A J 1996 Dynamics of tissue optics during laser heating of turbid media *Appl. Opt.* **35** 3413–20
- MacKenzie H A, Ashton H S, Spiers S, Shen Y C, Freeborn S S, Hannigan J, Lindberg J and Rae P 1999 Advances in photoacoustic noninvasive glucose testing *Clin. Chem.* **45** 1587–95
- Pesach B, Bitton G, Antebi A, Ben-David M and Nagar R 2004 Continuous non-invasive blood glucose monitor based on photoacoustic sensing technology *Abstracts from 4th Inter-Institute Workshop on Optical Diagnostic Imaging from Bench to Bedside at the National Institutes of Health 2004*
- Splinter R, Svenson R H, Littmann L, Tuntelder J R, Chuang C H, Tatsis G P and Thompson M 1991 Optical-properties of normal, diseased, and laser photocoagulated myocardium at the Nd-Yag wavelength *Lasers Surg. Med.* **11** 117–24
- Techavipoo U, Varghese T, Chen Q, Stiles T A, Zagzebski J A and Frank G R 2004 Temperature dependence of ultrasonic propagation speed and attenuation in excised canine liver tissue measured using transmitted and reflected pulses *J. Acoust. Soc. Am.* **115** 2859–65
- Thomsen S 1995 Identification of lethal thermal injury at the time of photocoagulation *Laser-Induced Interstitial Thermotherapy* ed G Muller *et al* (Bellingham, WA: SPIE) 459–67
- Wang L H V 2003 Ultrasound-mediated biophotonic imaging: a review of acousto-optical tomography and photo-acoustic tomography *Disease Markers* **19** 123–38
- Wang X D, Ku G, Wegiel M A, Bornhop D J, Stoica G and Wang L H V 2004 Noninvasive photoacoustic angiography of animal brains in vivo with near-infrared light and an optical contrast agent *Opt. Lett.* **29** 730–2
- Wang X D, Pang Y J, Ku G, Stoica G and Wang L H V 2003a Three-dimensional laser-induced photoacoustic tomography of mouse brain with the skin and skull intact *Opt. Lett.* **28** 1739–41
- Wang X D, Pang Y J, Ku G, Xie X Y, Stoica G and Wang L H V 2003b Noninvasive laser-induced photoacoustic tomography for structural and functional in vivo imaging of the brain *Nature Biotechnol.* **21** 803–6
- Wang X D, Xu Y, Xu M H, Yokoo S, Fry E S and Wang L H V 2002 Photoacoustic tomography of biological tissues with high cross-section resolution: reconstruction and experiment *Med. Phys.* **29** 2799–805
- Weast R C 1974 *Handbook of Chemistry and Physics* 54 edn, (Boca Raton, FL: CRC Press)
- Weidensteiner C, Quesson B, Caire-Gana B, Kerioui N, Rullier A, Trillaud H and Moonen C T W 2003 Real-time MR temperature mapping of rabbit liver in vivo during thermal ablation *Magn. Reson. Med.* **50** 322–30
- Welch A J and van Gemert M J C 1995 *Optical-Thermal Response of Laser-Irradiated Tissue* (New York: Plenum)